Supporting information

Chemical Control and Spectral Fingerprints of Electronic Coupling in Carbon Nanostructures

Jacek Kłos[†§], Mijin Kim[†§], Millard H. Alexander[†‡] and YuHuang Wang[*†#]

[†]Department of Chemistry and Biochemistry, [‡]Institute for Physical Science and Technology,

[#]Maryland NanoCenter, University of Maryland, College Park, Maryland 20742, United States

[§]J.K., M.K.: These authors contributed equally to this work.

[*]Correspondence should be addressed to Y.H.W. (yhw@umd.edu)

Supplementary Computational Methodology

Optimized geometries of studied core-shell complexes. We performed calculations for this work with the Amsterdam Density Functional 2014 (ADF) suite of codes.[1] The starting Cartesian coordinates for the C_{60}, C_{180}, C_{240}, C_{260} and C_{320} fullerenes were taken from Mitsuho Yoshida Fullerene Library.[2] The geometry of complexes were optimized at the BLYP-D3 level of theory with the double-ζ (DZ) basis set, where D3 denotes improved dispersion corrections of Grimme *et al.*[3] and Becke-Lee-Yang-Parr (BLYP) is a DFT functional as implemented in the ADF 2014 program. The geometry optimizations were converged at energy and gradient thresholds of $5^{*}10^{-5}$ and $5^{*}10^{-4}$ a.u., respectively. We noticed that the larger core-shell structures, such as $C_{60}@C_{320}$ and $C_{60}@C_{240}F_{240}$ posed problems in geometry convergence, due to larger separations between the inner C_{60} and the outer carbon layer and the Mexican hat type of potential (see the main text) along the radial coordinate placing the saddle point in the center of origin of system of coordinates. To reduce the computational cost, we increased the convergence thresholds to 10 times higher. The calculation was continued until the spectral features of slightly different geometries barely changed over the iterations, as shown in Figure S1. For the geometry optimization of $C_{60}@C_{320}H_{320}$ and $C_{60}@C_{320}F_{320}$, the outer shells were pre-optimized with the static variant of Merck molecular force field 94 (MMFF94s)[4] in the Avogadro[5] program and then the obtained coordinates were imported to construct the core-shell complexes. MMFF94s can be applicable in fullerene core-shell structures because this model describes well conformational, intra- and intermolecular interactions. To reduce the computational cost to a reasonable level, the core-shell complexes were optimized keeping the outer-shell geometry fixed using a BLYP-D3/DZ basis.

Inter-particle electronic transitions. The UV-Visible absorption spectra of isolated structures and core-shell complexes considered in this work have been calculated from singlet-singlet electronic transitions using the time-dependent density functional tight binding (TD-DFTB) method[6] with the Quasinano2013.1 parameter set[7] implemented in the ADF package. The time-dependent approach allows for the calculations of the excited states within the approach of the linear response (first-order in the perturbation) in DFT that leads to the eigenvalue problem spanned by single excitations (singlet-singlet or singlet-triplet). Linear response theory calculates the first order effect of the external perturbation to the Hamiltonian assuming the perturbation is weak and doesn't affect the ground state significantly. The linear response function only retains

the first linear term in the expansion around the ground state density. While regular TD-DFT is computationally expensive and limited in application to moderately-sized molecules, the tight binding approximations in the TD-DFTB approach use only two-center integrals, which allow excited states calculations with great computational speed-up and without the loss of major spectral features. The Quasinano2013.1 parameter set used in the tight binding approximation of two-center Hamiltonian matrix elements in the DFT expressions is optimized to cover most of the periodic table including C, H, and F involved in this study.[7] We note that Quasinano2013.1 TD-DFT HOMO orbitals for the perfluorinated compounds are comparable to canonical Hartree-Fock orbitals than the Kohn-Sham orbitals from full DFT calculations. More specifically, HOMO of perfluorinated compound in tight-binding DFT calculations is located on the C_{60}, while in Kohn-Sham DFT calculations it is located on the outside perfluorinated shell.

Our methodology is supported by a direct comparison of calculated UV-visible spectra of C_{60} with experimentally determined data[8] (Figure S2). We have also considered the effects of basis sets for the geometry optimization. Both DZ and larger basis set of triple-zeta quality (TZP) give practically the same results from the spectral calculations of C_{60}@C_{240} (Figure S3) and our calculations agree well with the experimental measurement.

Geometry Optimization Convergence Test in a Large System

The time-dependent tight-binding DFT method (TD-DFTB) (with no dispersion corrections added) is employed for the geometries optimized using the BLYP-D3/DZ approach. The UV-Visible spectra are generated from 9000 singlet and triplet excitations using Davidson diagonalization in the ADF program. To confirm the convergence of the optimized geometry, the UV-Visible absorption spectra of the 6 iterations are compared. As shown in Figure S1, all UV-Visible spectra of slightly different $C_{60}@C_{320}$ geometries are very similar. This indicates that at these iterations, the geometry is almost converged to an optimized level, giving rise to consistent spectral profiles and theoretical results.

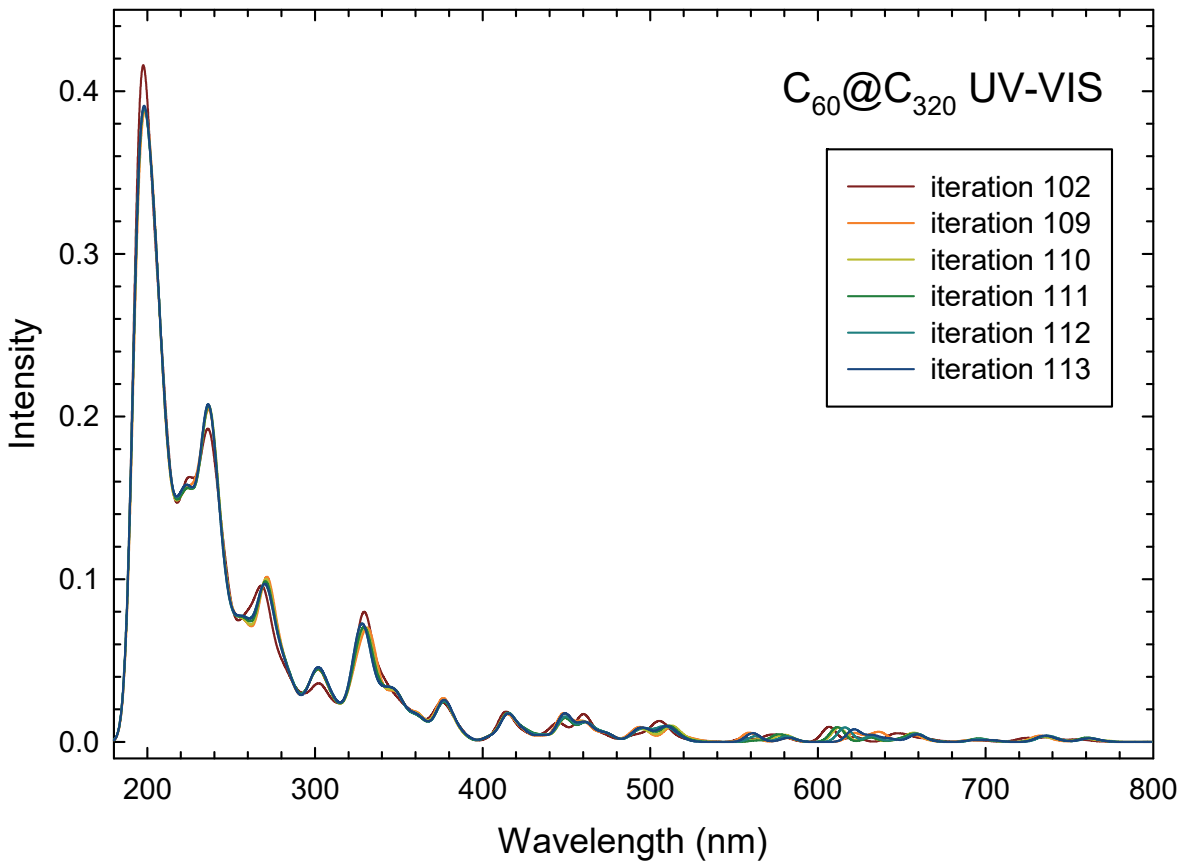

Figure S1. Iterated calculations of UV-visible absorption spectra of $C_{60}@C_{320}$ confirm convergence of calculation.

UV-Visible spectra of free C_{60}: Experimental vs. Calculated

The geometry optimized C_{60} using BLYP-D3/DZ is used for UV-visible excitation calculation using the TD-DFTB method with Quasinano2013.1 parameter set. The calculated spectrum was further Gaussian convoluted with fwhm of 10 nm to mimic broadening effects occurring under experimental conditions. The calculated UV-Vis spectrum is compared with the experimental data obtained from C_{60} in n-heptane.[8] As shown in Figure S2, the calculated spectrum is in reasonable agreement with the experiment.

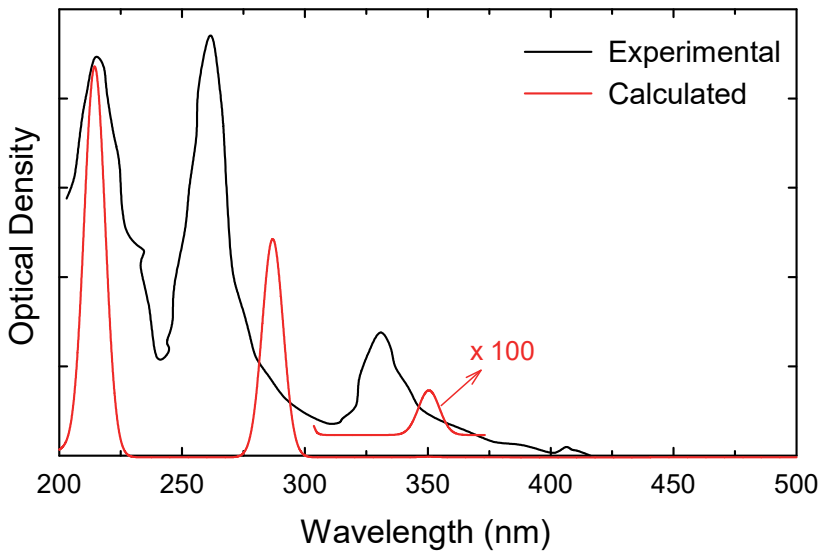

Figure S2. UV-Vis spectra of C_{60}: experiment (in n-heptane) vs. calculation (in vacuum)

IR spectra of free C_{60}: Experimental vs. Calculated

We calculated the infrared spectrum of C_{60} after geometry optimization using BLYP-D3/DZ approach in the ADF program. The calculated IR spectrum is compared with the experimental data obtained from C_{60} thin films[9] in Figure S3. The calculated spectrum has four distinct bands, with a single more intense feature in the region of the 500 cm^{-1}, in good agreement with the experiment. There is a red shift of ~40 cm^{-1} for the calculated frequencies at ~1170 and ~1450 cm^{-1} in comparison with the experimental values. This small discrepancy may arise from the accuracy of theory or the fact that experimental data is collected from thin films involving intermolecular interactions whereas our calculation considers isolated C_{60} molecules in vacuum.

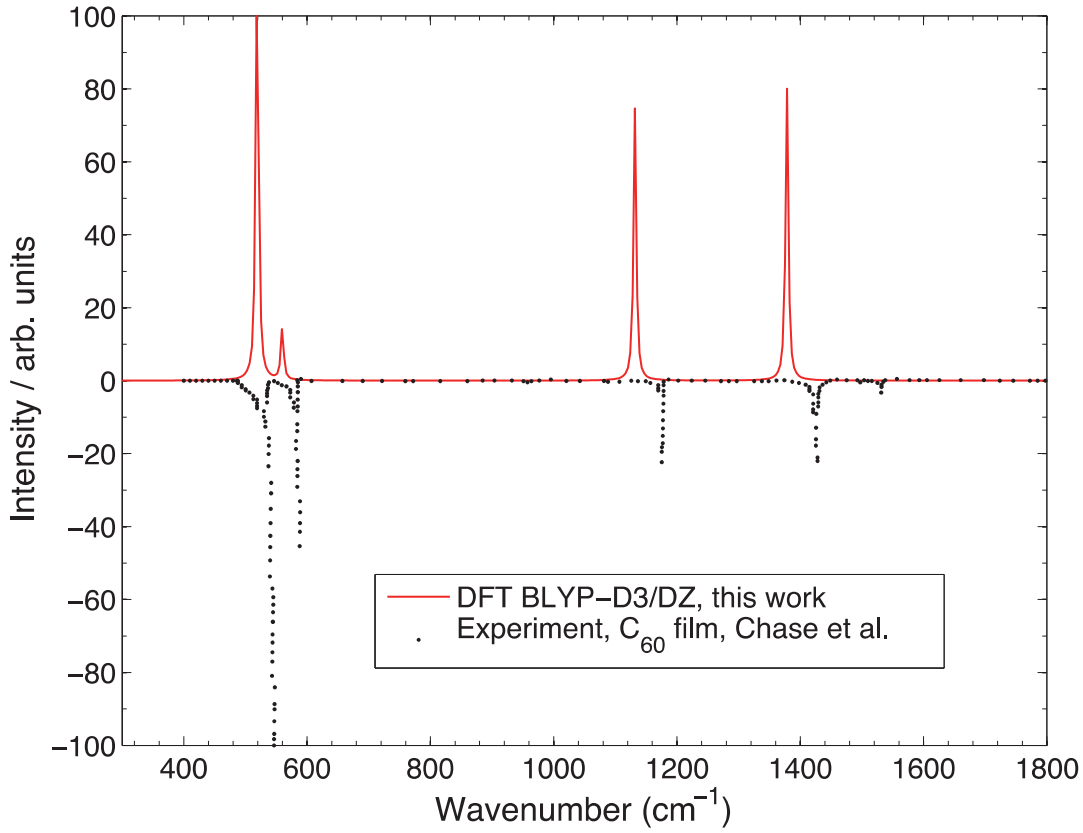

Figure S3. Infrared spectra of C_{60}: experiment vs. calculation.

UV-Visible Absorption Spectra: The Effect of Basis Set

To investigate the effect of basis set on the electronic structures of studied complexes, we have repeated the TD-DFTB calculations (with no dispersion corrections added) with DZ and TZP basis sets. The UV-Visible spectra are generated from 9000 singlet and triplet excitations using Davidson diagonalization in the ADF program. Figure S4 compares the two UV-Visible spectra of C_{60}@C_{240} obtained with DZ and TZP basis sets. Both basis sets provide very similar spectral features including peak position and intensity, justifying the use of the smaller DZ basis for the geometry optimization in this study.

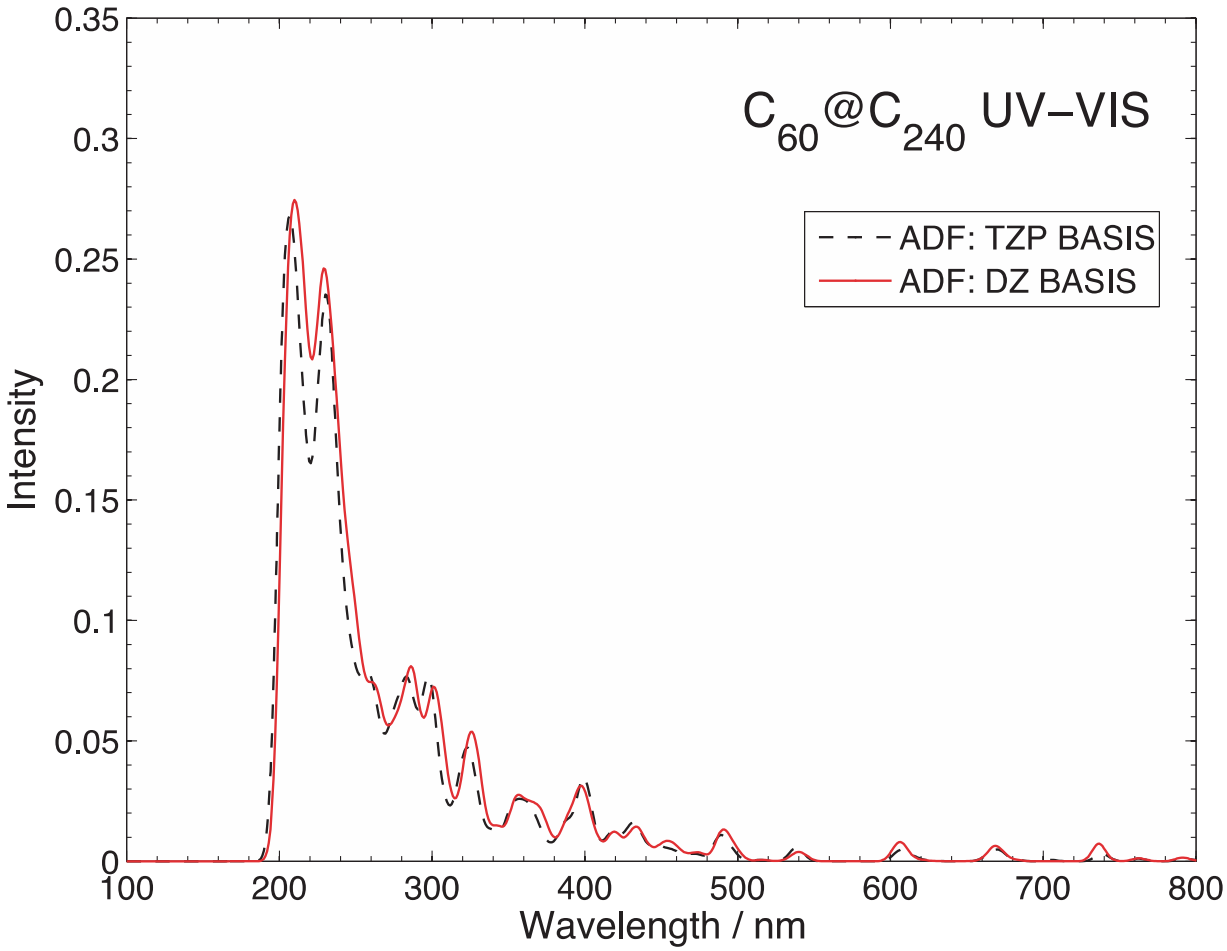

Figure S4. UV-visible spectra of C_{60}@C_{240} obtained with DZ and TZP basis sets.

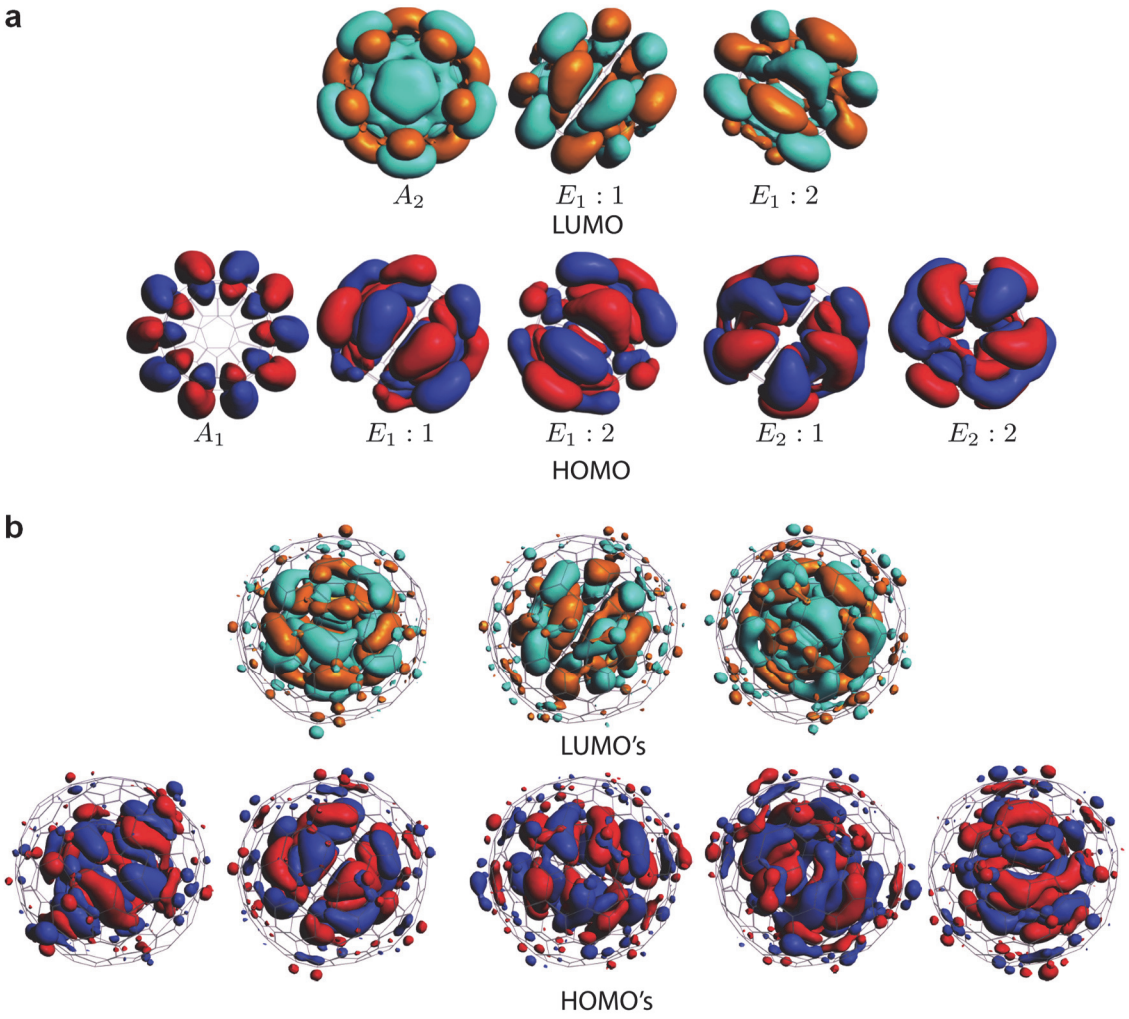

Figure S5. The set of five HOMOs and three LUMOs for (a) free C_{60} and (b) C_{60} in $C_{60}@C_{180}$ obtained from the DFT BLYP-D3/DZ calculations. While the HOMOs and LUMOs of C_{60} fullerene correspond to five-fold and three-fold degenerate energies,[9] the HOMO and LUMO degeneracy of the icosahedral (I_h) complex is broken due to intermolecular interactions. Isoorbital value is set to 0.01.

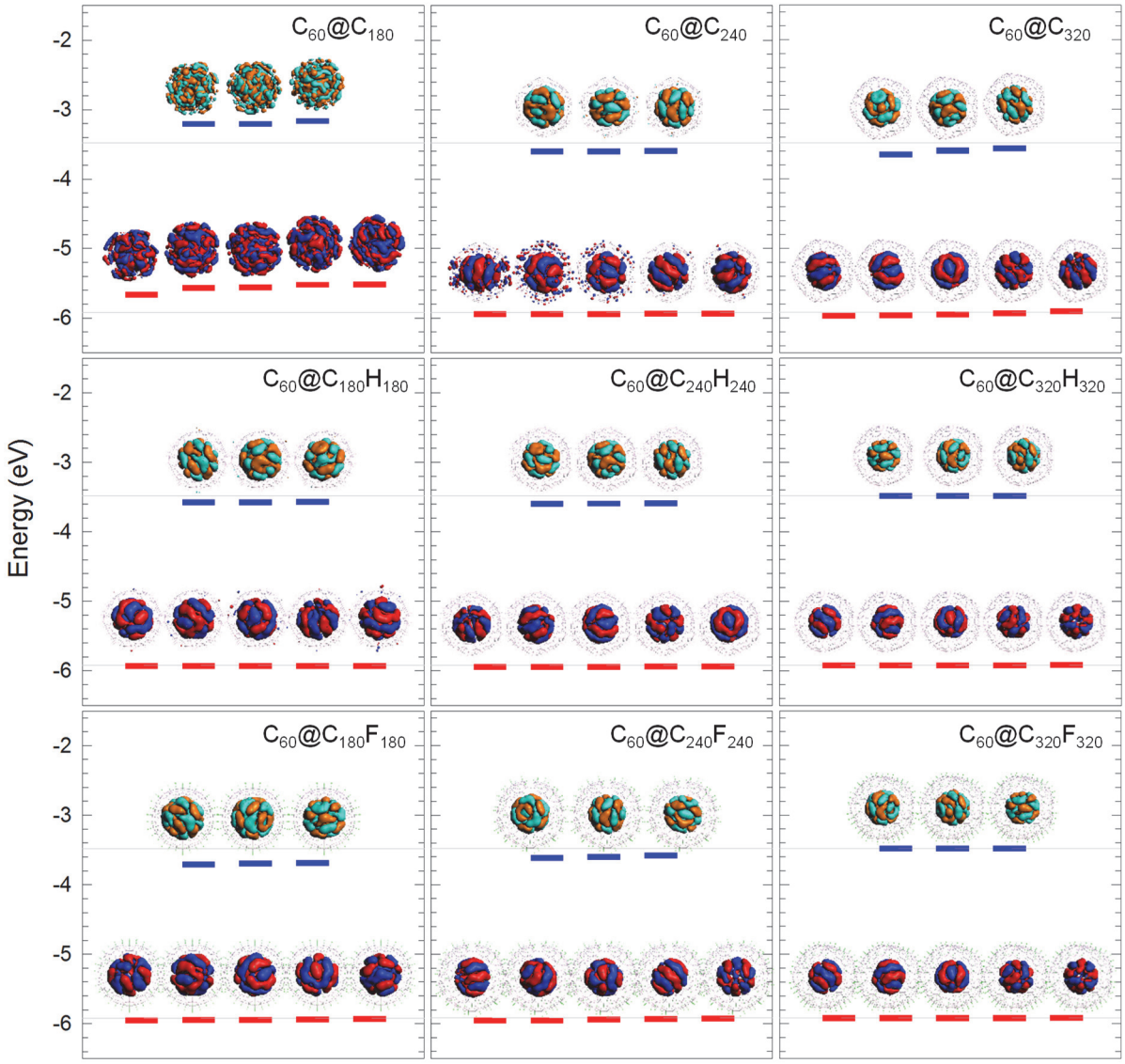

Figure S6. The set of orbitals and energy levels of five HOMOs (red lines) and three LUMOs (blue lines) of C_{60} in the core-shell complexes obtained from the TD-DFTB Quasinano2013.1 calculations. The gray guide lines are the frontier orbital energy levels of a free C_{60} (the HOMO-LUMO electron density distribution for an isolated C_{60} is shown in Figure S1). Iso-orbital value is set to 0.003.

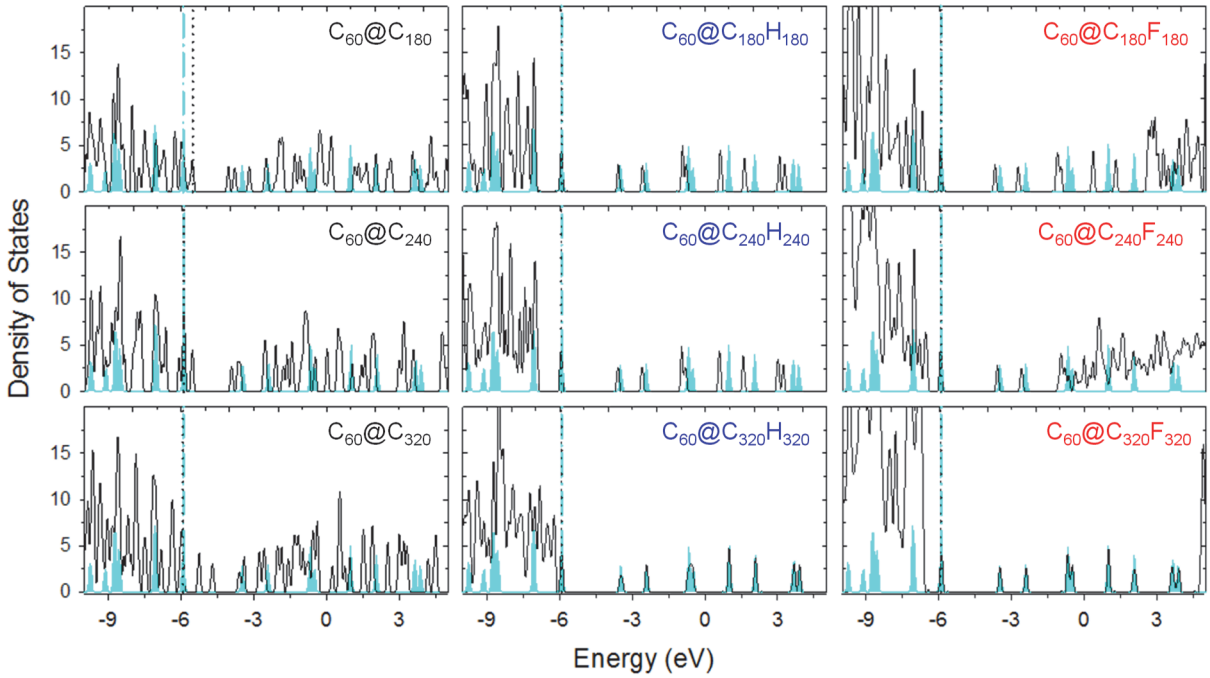

Figure S7. The density of states for free C_{60} (blue background) and core-shell complexes, $C_{60}@C_{180}$ (top), $C_{60}@C_{240}$ (middle), $C_{60}@C_{320}$ (bottom). The spectra are calculated by the TD-DFTB method with Quasinano2013.1 parameter set and simulated using a Gaussian convolution with 0.5 eV fwhm to mimic the broadening effects in experimental measurements. Depending on the surface functionality and dimension of the outer layer, both occupied and virtual state distributions substantially change. Dashed lines indicate Fermi level of free C_{60} (blue) and core-shell complexes (black).

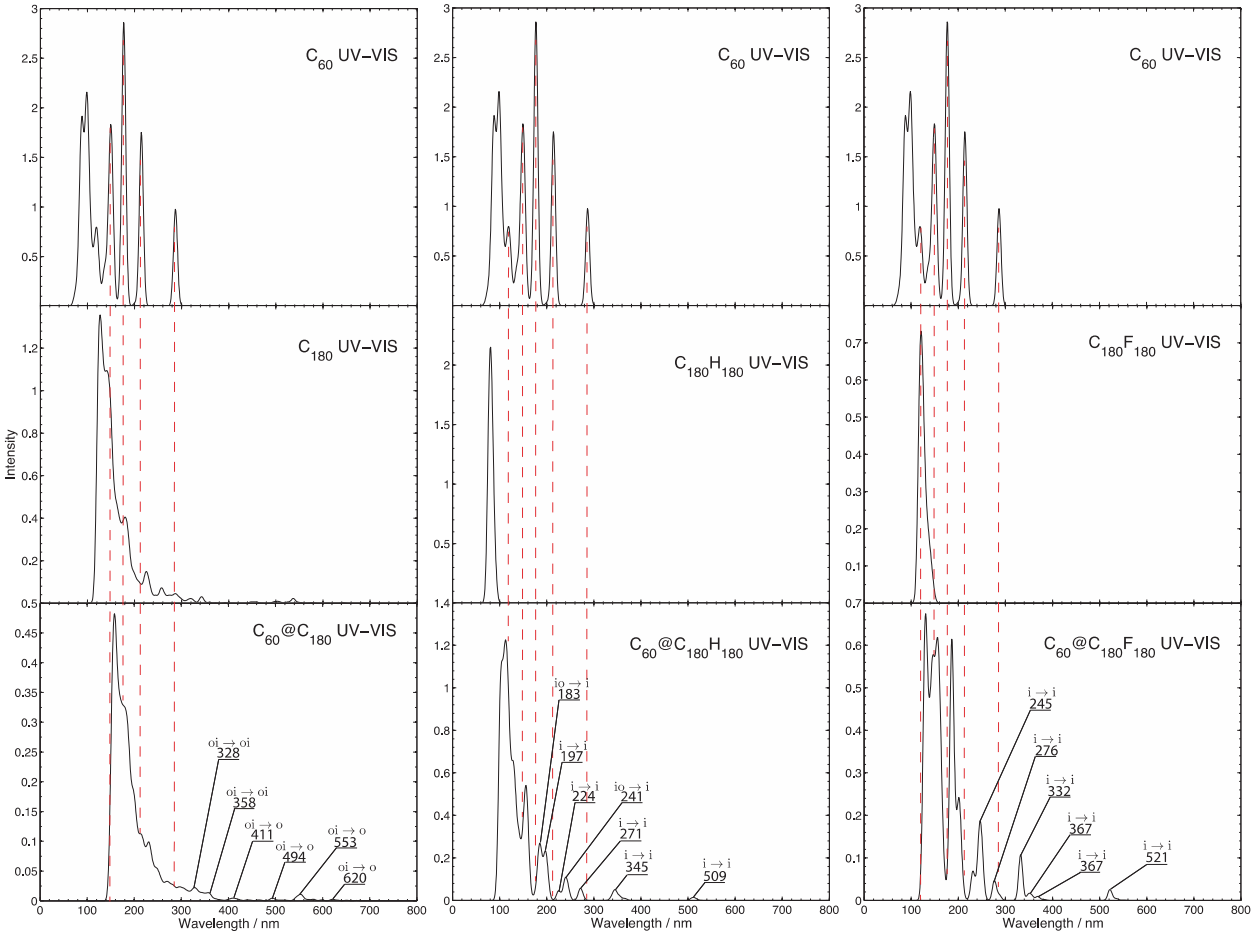

Figure S8. Calculated UV-Visible absorption spectra of C_{60} (top row), C_{180} (middle left), $C_{180}H_{180}$ (middle center), $C_{180}F_{180}$ (middle right), and the core-shell structures: $C_{60}@C_{180}$ (bottom left), $C_{60}@C_{180}H_{180}$ (bottom center) and $C_{60}@C_{180}F_{180}$ (bottom right). The excitation spectra are calculated using the TD-DFTB method with Quasinano2013.1 parameter set and assume a Gaussian convolution with fwhm of 10 nm. The dashed lines show positions of the peaks in the spectra of C_{60}. In the bottom row we indicate wavelengths of the major transitions (with the largest oscillator strength) contributing to each spectral peak in the low excitation energy region. We also mark the major composition of each transition if it occurs between the inner (i) and outer (o) layer, or within the same layer. For orbitals that extend over the core and shell layers, the label of 'io' (or 'oi') is used where the major contribution is from the inner (or outer) layer.

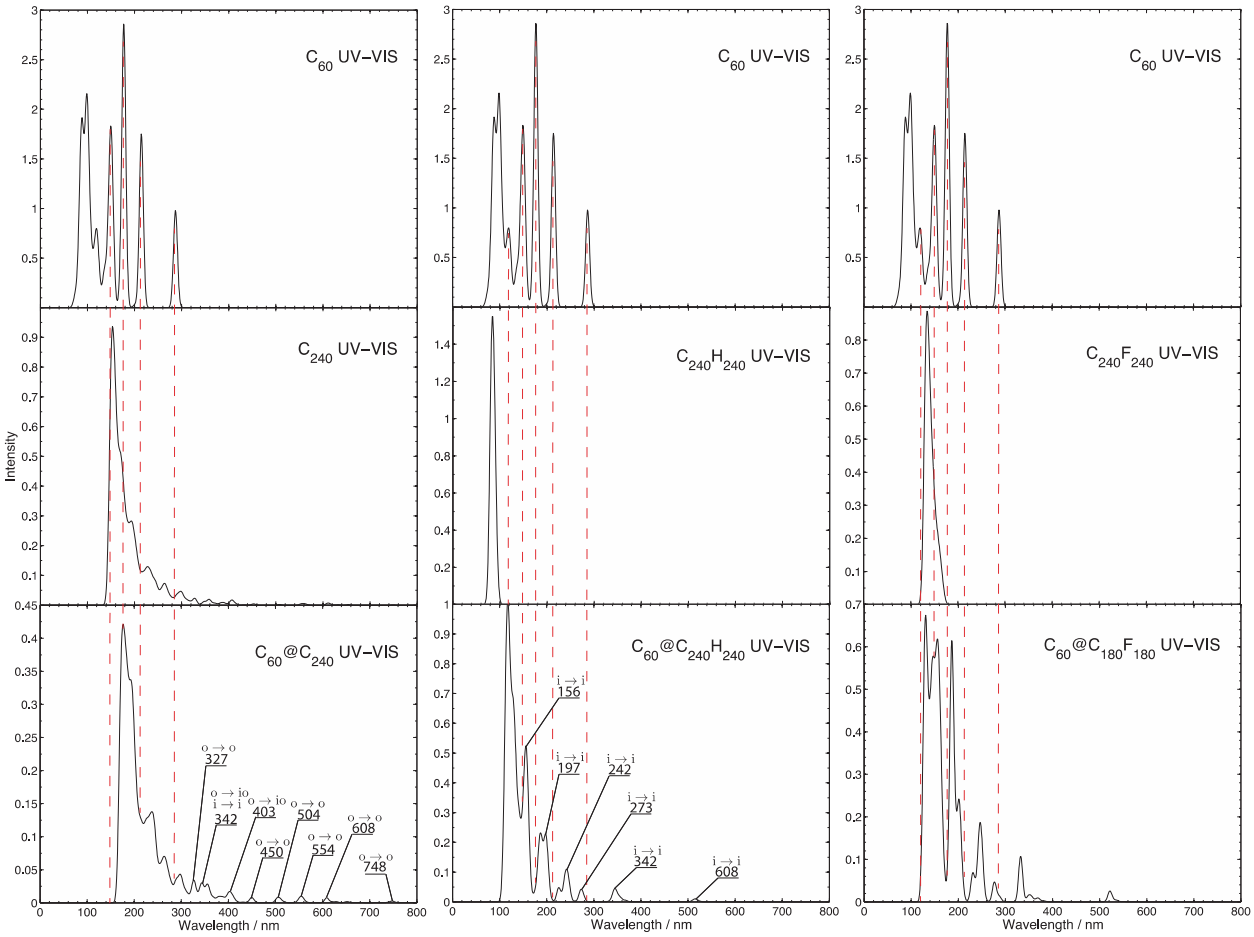

Figure S9. Calculated UV-Visible spectra of C_{60} (top row), C_{240} (middle left), $C_{240}H_{240}$ (middle center), $C_{240}F_{240}$ (middle right), and the core-shell structures: $C_{60}@C_{240}$ (bottom left), $C_{60}@C_{240}H_{240}$ (bottom center) and $C_{60}@C_{240}F_{240}$ (bottom right). The excitation spectra are calculated using the TD-DFTB method with Quasinano2013.1 parameter set and assume a Gaussian convolution with fwhm of 10 nm. The dashed lines show positions of the peaks in the spectra of C_{60}. In the bottom row we indicate wavelengths of the major transitions (with the largest oscillator strength) contributing to each spectral peak in the low excitation energy region. We also mark the major composition of each transition if it is between the inner (i) and outer (o) layer, or within the same layer. For orbitals that extend over the core and shell layers, the label of 'io' (or 'oi') is used where the major contribution is from the inner (or outer) layer.

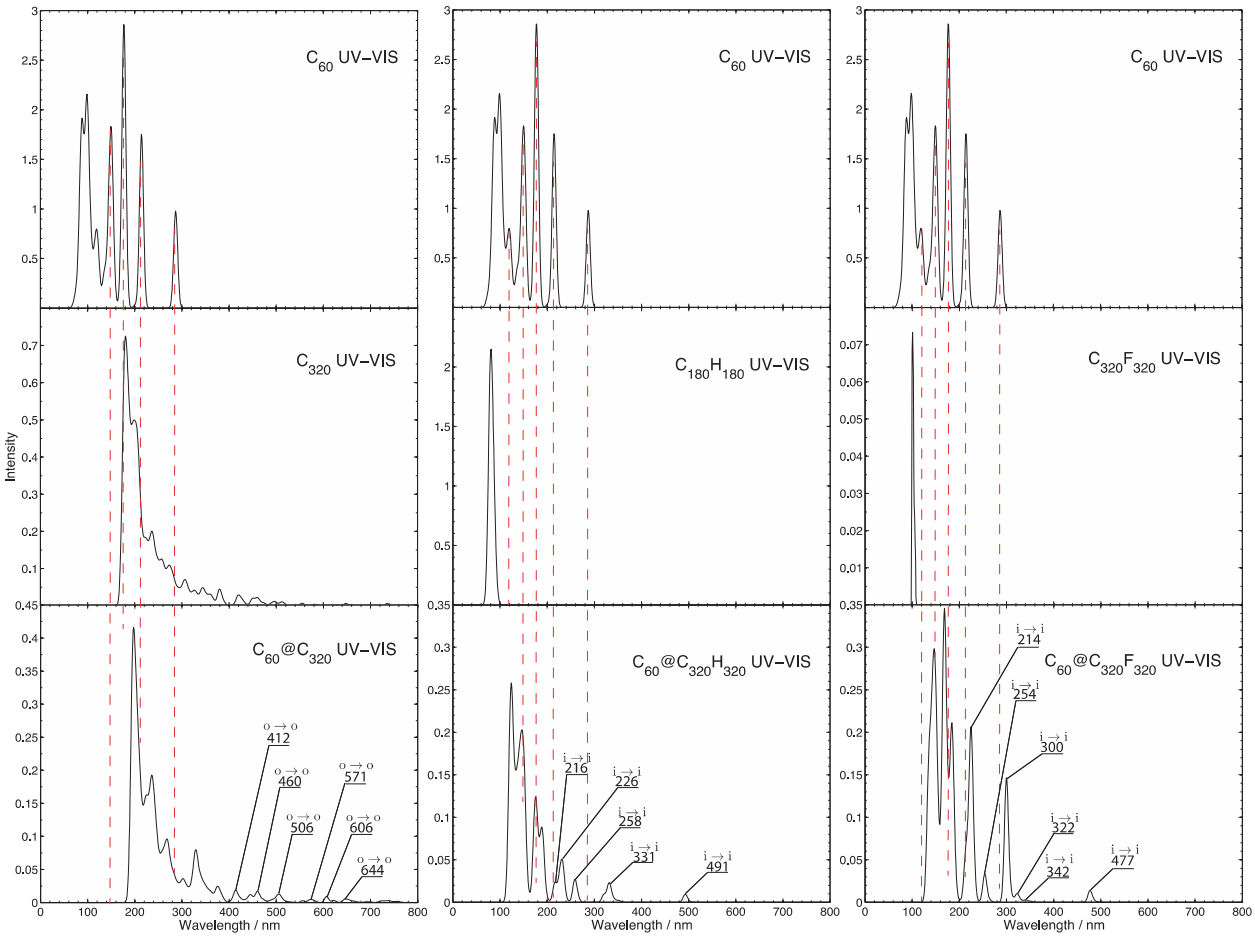

Figure S10. Calculated UV-Visible spectra of C_{60} (top row), C_{320} (middle left), $C_{320}H_{320}$ (middle center), $C_{320}F_{320}$ (middle right), and the double-layer structures: $C_{60}@C_{320}$ (bottom left), $C_{60}@C_{320}H_{320}$ (bottom center) and $C_{60}@C_{320}F_{320}$ (bottom right). The excitation spectra are calculated using the TD-DFTB method with Quasinano2013.1 parameter set and assume a Gaussian convolution with fwhm of 10 nm. The dashed lines show positions of the peaks in the spectra of C_{60}. In the bottom row we indicate wavelengths of the major transitions (with the largest oscillator strength) contributing to each spectral peak in the low excitation energy region. We also mark the major composition of each transition if it is between the inner (i) and outer (o) layer, or within the same layer. For orbitals that extend over the core and shell layers, the label of 'io' (or 'oi') is used where the major contribution is from the inner (or outer) layer.

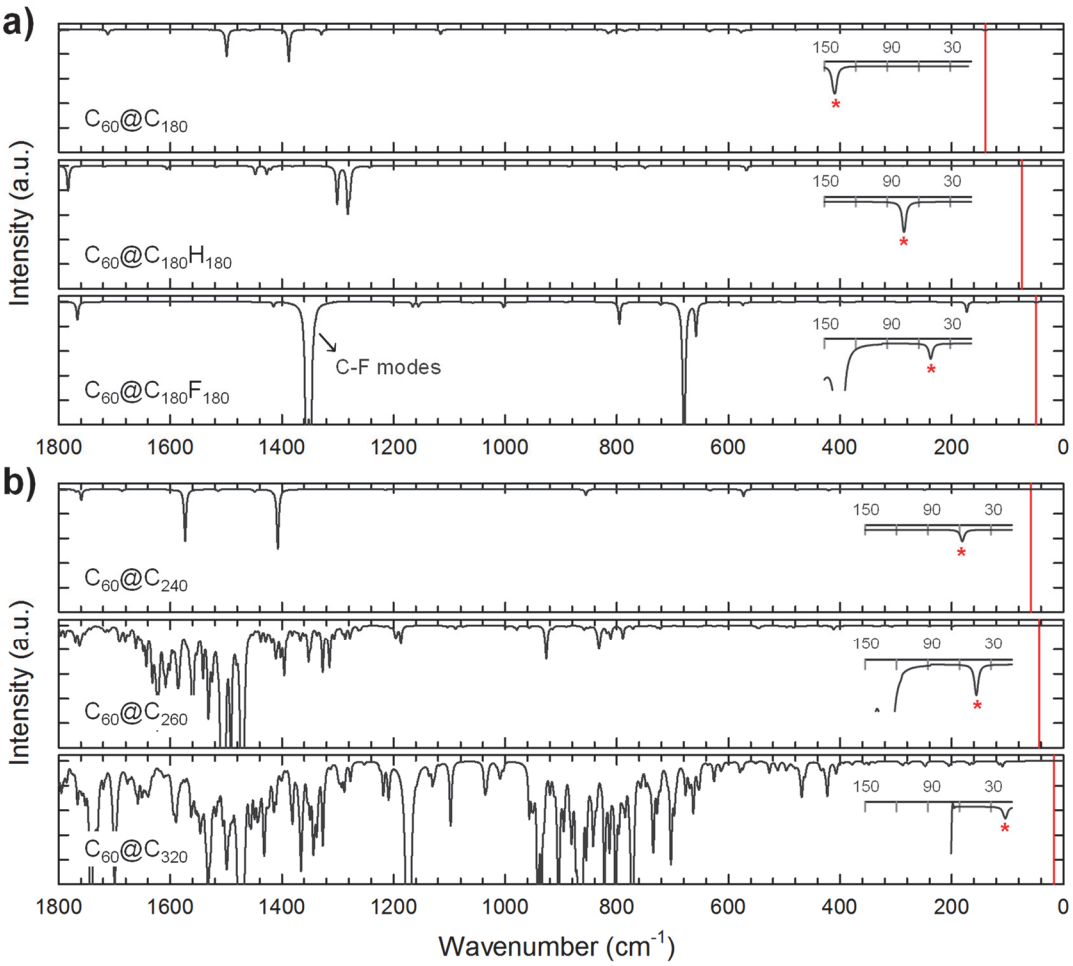

Figure S11. Infrared (IR) spectra of core-shell complexes with fwhm of 2 cm^{-1}, calculated using semiempirical Austin model (AM1) method,[10] implemented in Gaussian 09.[11] The peak corresponding to the C_{60} oscillatory motion is indicated with a red guide line and asterisk (*). The insert plots are zoomed into the frequency region of 10 to 150 cm^{-1}. As a core-shell structure becomes decoupled by (a) chemical functionalization of a shell or by (b) increasing inter-layer distance, the C_{60} oscillatory frequency is lower. The IR intensity of $C_{60}@C_{180}F_{180}$ is divided by a factor of 3 for clarity.

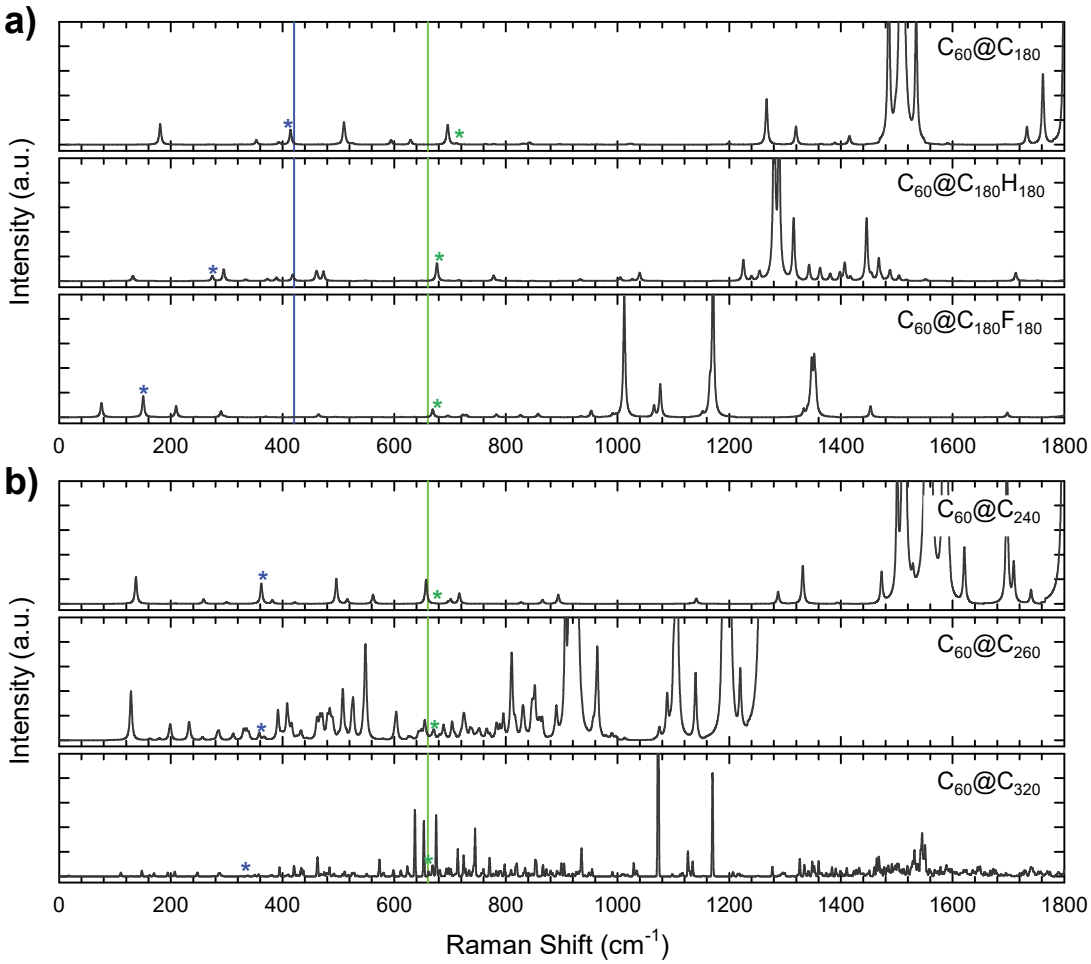

Figure S12. Calculated Raman spectra of core-shell complexes. The method used is Gaussian 09 AM1. The peaks are convoluted with a fwhm of 2 cm^{-1}. The blue and green guide lines represent radial breathing modes (RBM) of free C_{60} and C_{180}, respectively. The RBMs of core and shell of the complexes are marked by asterisks. As the core-shell structure becomes decoupled by (a) chemical functionalization of shell or by (b) increasing inter-layer distance, the RBM peak position of C_{60} becomes closer to that of the free C_{60}. The peak corresponding to the C_{60} rotational motion inside the complex (at 5 - 100 cm^{-1}) is Raman active but with very low intensity. Note that the intensity of $C_{60}@C_{180}H_{180}$, $C_{60}@C_{180}F_{180}$ are magnified by a factor of 10 and that of $C_{60}@C_{320}$ is reduced by a factor of 50 for clarity.

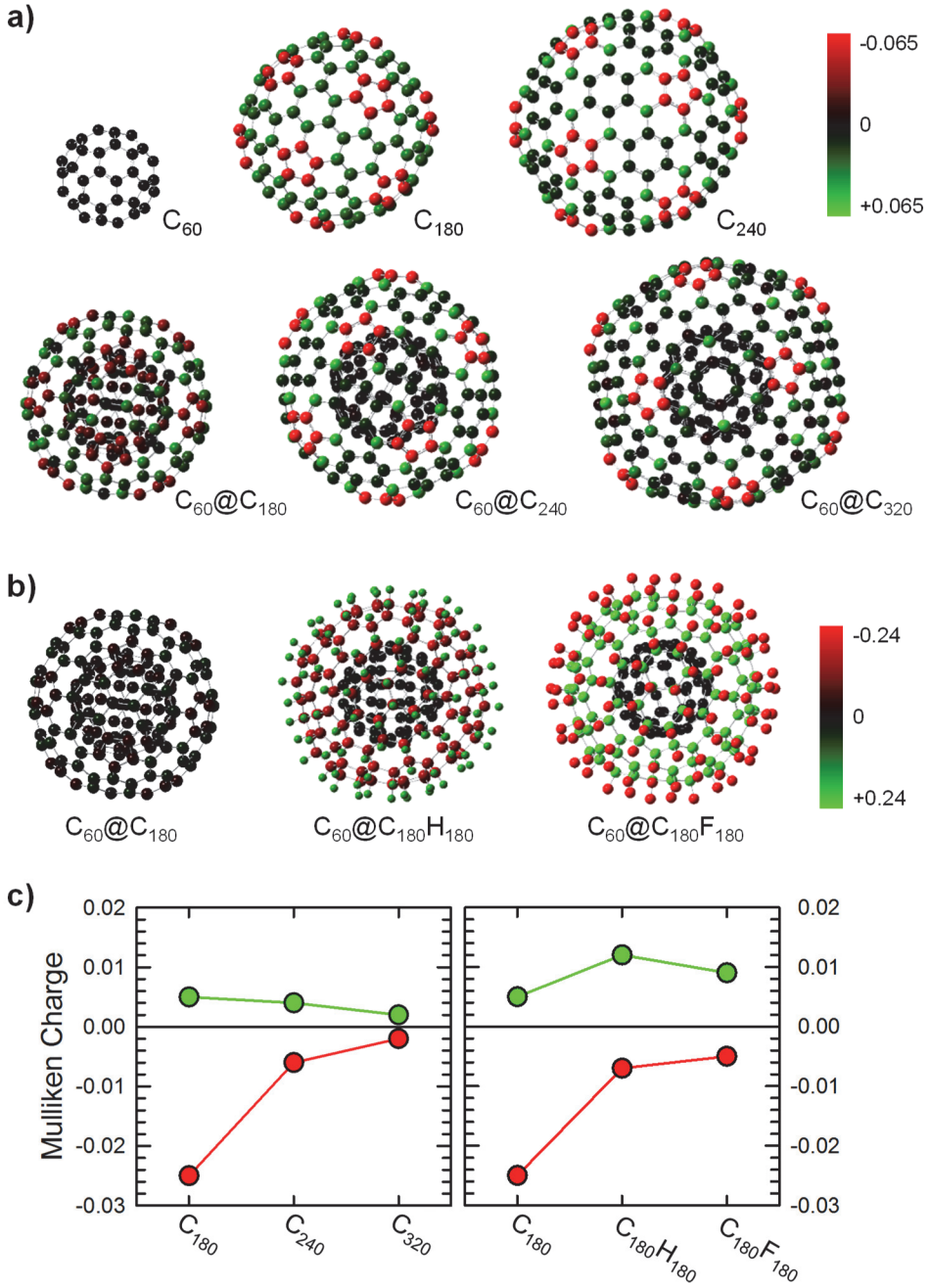

Figure S13. Mulliken analysis of charge as a function of (a) the outer shell size and (b) the surface functionality of C_{60}@C_{180}. Compared to free C_{180}, the outer shell carbons in C_{60}@C_{180} show a similar pattern in charge distribution but the density becomes lower. With large shells, as in C_{240}, the charge distribution in the shell is identical, in both pattern and strength, to its free form. Upon surface functionalization, the Mulliken charge of C_{180} shell is significantly altered. (c) In contrast to zero local charge in free C_{60}, the Mulliken charge of encapsulated C_{60} can build up depending on the chemical environment. The maximum strength of positive (green circles) and negative (red circles) charges are presented. Note that the net charge of the inner C_{60} is negative (or positive) as it is encapsulated by a sp^2 (sp^3) shell.

Table S1. Structural parameters. (**a**) Radii for a free C_{60}, and C_{60} inner carbon sphere of core-shell complexes (**b**) Radii for C_{180}, C_{240}, C_{320}, and the shell of core-shell complexes. The structures are optimized at the BLYP-D3/DZ level with dispersion corrections. The radius is defined as the average distance of carbon atoms from the center of the system ($\bar{r}$). *Note that $C_{320}H_{320}$ and $C_{320}F_{320}$ are pre-optimized by MMFF94s force field[5] in the Avogadro software[5] and the geometry optimization for $C_{60}@C_{320}H_{320}$ and $C_{60}@C_{320}F_{320}$ are performed with the shell conformation frozen. Subscript x denotes the number of shell atoms (180, 240 or 320, respectively).

a)

	r_{C60} / Å		
	C_{180}	C_{240}	C_{320}
C_{60} in C_x	3.514	3.596	3.595
C_{60} in $(CH)_x$	3.587	3.592	3.587*
C_{60} in $(CF)_x$	3.623	3.472	3.579*
C_{60} isolated	3.544		

b)

	r_{outer} / Å		
	C_{180}	C_{240}	C_{320}
C_x	6.179	7.132	8.127
$(CH)_x$	6.896	7.743	8.861*
$(CF)_x$	7.513	8.858	9.321*
C_{60} in C_x	6.276	7.116	8.203
C_{60} in $(CH)_x$	6.882	7.961	8.861*
C_{60} in $(CF)_x$	7.383	7.996	9.321*

Table S2. Core-shell separations. The structures are optimized at the BLYP-D3/DZ level with dispersion corrections. The core-shell separation, ξ is defined as $\bar{r}_{\text{outer}} - \bar{r}_{\text{inner}}$. In parenthesis we give the shortest C-C distance between a carbon atom in the core and another in the shell. *Note that $C_{320}H_{320}$ and $C_{320}F_{320}$ are pre-optimized by MMFF94s force field in Avogadro and the geometry optimization for $C_{60}@C_{320}H_{320}$ and $C_{60}@C_{320}F_{320}$ are performed with frozen shell conformation. Subscript x denotes the number of shell atoms (180, 240 or 320, respectively).

	ξ / Å		
	C_{180}	C_{240}	C_{320}
C_{60} in C_x	2.762 (2.689)	3.52 (3.373)	4.608 (4.386)
C_{60} in $(CH)_x$	3.295 (3.187)	4.369 (4.179)	5.274* (5.009)
C_{60} in $(CF)_x$	3.76 (3.679)	4.524 (4.283)	5.742* (5.497)

Table S3. Frontier orbital energies of free and encapsulated C_{60} core and band gaps (E_g) of the core-shell structures are listed. The energies are calculated with Quasinano2013.1 DFTB parameters.

Unit: eV

System	HOMO	LUMO	E_g	HOMO-LUMO gap of C_{60}
C_{60}	-5.918	-3.480	2.438	2.438
$C_{60}@C_{180}$	-5.518	-4.073	1.445	2.313
$C_{60}@C_{240}$	-5.576	-3.951	1.624	2.340
$C_{60}@C_{320}$	-4.762	-4.713	0.049	2.343
$C_{60}@C_{180}H_{180}$	-5.929	-3.578	2.351	2.362
$C_{60}@C_{240}H_{240}$	-5.935	-3.709	2.226	2.348
$C_{60}@C_{320}H_{320}$	-5.940	-3.597	2.343	2.438
$C_{60}@C_{180}F_{180}$	-5.927	-3.614	2.313	2.248
$C_{60}@C_{240}F_{240}$	-5.918	-3.480	2.438	2.438
$C_{60}@C_{320}F_{320}$	-5.918	-3.480	2.438	2.313

Supplementary References

1. Baerends, E.J.; Ziegler, T.; Autschbach, J.; Bashford, D.; Bérces, A.; Bickelhaupt, F.M.; Bo, C.; Boerrigter, P.M.; Cavallo, L.; Chong, D.P. *et al. ADF 2014*; Software for Chemistry & Materials: Amsterdam, The Netherlands, 2014.
2. Yoshida, M. Fullerene Library, *http://www.cochem2.tutkie.tut.ac.jp/Fuller/Fuller.html*
3. Grimme, S.; Antony, J.; Ehrlich, S.; Krieg, H. A Consistent and Accurate Ab Initio Parametrization of Density Functional Dispersion Correction (DFT-D) for the 94 Elements H-Pu. *J. Chem. Phys.* **2010**, *132*, 154104.
4. Halgren, T. A. Merck Molecular Force Field. I. Basis, Form, Scope, Parameterization, and Performance of MMFF94. *J. Comput. Chem.* **1996**, *17*, 490-519.
5. Hanwell, M.; Curtis, D.; Lonie, D.; Vandermeersch, T.; Zurek, E.; Hutchison, G. Avogadro: An Advanced Semantic Chemical Editor, Visualization, and Analysis Platform. *J. Cheminform.* **2012**, *4*, 17.
6. Yakovlev, A.; Philipsen, P.; Borini, S.; Rüger, R.; de Reus, M.; Ghorbani-Asl, M.; McCormack, D.; Patchkovskii, S.; Heine. T. *ADF DFTB 2014*; Software for Chemistry & Materials: Amsterdam, The Netherlands, 2014.
7. Wahiduzzaman, M.; Oliveira, A.F.; Philipsen, P; Zhechkov, L.; van Lenthe, E.; Witek, H.A.; Heine, T. DFTB Parameters for the Periodic Table: Part 1, Electronic Structure. *J. Chem. Theory Comput.* **2013**, *9*, 4006-4017.
8. Catalán. Towards the Gas-Phase UV-VIS Absorption Spectrum of C_{60}. *Chem. Phys. Lett.* **1994** *223*, 159-161.
9. Chase, B.; Herron, N.; Holler, E. Vibrational Spectroscopy of Fullerenes (C_{60} and C_{70}). Temperature Dependent Studies. *J. Phys. Chem.* **1992**, *96,* 15491.
10. Ozaki, M.A.; Taahashi, A. On Electronic States and Bond Lengths of the Truncated Icosahedral C_{60} Molecule. *Chem. Phys. Lett.* **1986**, *127*, 242-244.
11. Dewar, M.J.; Zoebisch, E.G.; Healy, E.F.; Stewart, J.J. Development and Use of Quantum Mechanical Molecular Models. 76. AM1: A New General Purpose Quantum Mechanical Molecular Model. *J. Am. Chem. Soc.* **1985**, *107*, 3902-3909.
12. Frisch, M. J.; Trucks, G. W.; Schlegel, H. B.; Scuseria, G. E.; Robb, M. A.; Cheeseman, J. R.; Scalmani, G.; Barone, V.; Mennucci, B.; Petersson, G. A. *et al. Gaussian 09*; Gaussian, Inc.: Wallingford, CT, USA, 2009.